A New Discrimination Method of Imaging Regions for Improved Ultrafast Ultrasound Imaging Performance

Shahad A. Thanoon*, Zainab Alomari, and Mahmod A. Al-Zubaidy
Electronics Engineering College, Ninevah University, Mosul 41002, Iraq

***e-mail:** shahad.abdulsalaam2021@stu.uoninevah.edu.iq

Abstract. Up to date, adaptive beamforming technologies have been successfully introduced to medical ultrasound imaging, resulting in a considerable improvement in imaging quality versus non-adaptive delay-and-sum beamformers. Minimum Variance (MV) adaptive beamforming improved resolution rather than contrast. At the same time, Eigen Space Based Minimum Variance (ESBMV) was formerly projected to enhance contrast in MV, but at the expense of the appearance of black regions around hyperechoic targets. Partial ESBMV (PESBMV) method has recently controlled the appearance of these black regions with a little reduction in the level of contrast. In this paper, a new technique of beamformer is proposed to improve the imaging quality of PESBMV. This approach uses two factors as a detection tool to adaptively indicate the regions of the image, then it applies the suitable beamforming method in each region. The results show that lateral resolution increased by 52% compared to that in PESBMV. Moreover, the contrast ratio is also increased with the preservation of the homogeneity of the background speckle. The proposed method is compared to MV, ESBMV, and PESBMV using *in vitro* experimental radio frequency data, showing improvement in the speckle preservation without affecting lateral resolution, and finally providing excellent image contrast performance. © 2023 Journal of Biomedical Photonics & Engineering.

Keywords: ultrasound imaging; plane wave imaging; minimum variance; eigenspace-based minimum variance; partial eigenspace-based minimum variance.

Paper #8982 received 24 May 2023; revised manuscript received 8 Sep 2023; accepted for publication 8 Sep 2023; published online 16 Dec 2023. doi: 10.18287/JBPE23.09.040310.

1 Introduction

Ultrasonography has been applied for imaging the body of humans for more than 50 years. The Austrian neurologist was the first to use ultrasonography as a medical diagnostic tool to see the head [1, 2]. As a diagnostic instrument, imaging in ultrasound is one of the most common imaging technologies in the medical imaging field [2]. Medical ultrasound imaging has been introduced for a variety of applications over the last few decades, and its capabilities have been expanded beyond the traditional B-mode and Doppler functions, shear-wave elastography, and other advanced applications [3] as well as mapping of ultrafast blood flow [4]. It is portable, radiation-free, and very affordable in comparison to other imaging technologies, like computed tomography and magnetic resonance. In addition, ultrasound images are tomographic, i.e., present a "cross-sectional" view of anatomical structure [2]. In the field of medical ultrasound, researchers and engineers searched to enhance image quality and frame rates [5, 6]. Plane wave imaging (PWI) is a form of imaging in which an unfocused single beam is utilized to visualize the imaging region. PWI creates a complete image with each transmission. Consequently, a high frame rate is incorporated in PWI composed of several thousand frames per second [7, 8]. Using the principle of PWI, which has been integrated into most sectors of medical ultrasonography, this field has undergone the revolution [6, 9]. Beamforming is the process of creating

an image from ultrasound echo signals generated from each array element [8]. This process is the most crucial step in revealing the information that passed reflected echo signals, otherwise, the ultrasound imaging procedure is meaningless [8]. Image quality in ultrasonography, specifically resolution, and contrast, is affected by the properties of the beam [10, 11]. The beamformer's main purpose is to generate a beam with reduced side lobes, on a depth, as well as a narrow main lobe [11, 12]. Regrettably, these are two contradictory objectives. The width of the main lobe affects the resolution of the image, while image contrast is determined by the sidelobe level and influences the dynamic range of image visualization [11].

The delay and sum (DAS) beamforming algorithm is the criterion technique for image reconstruction but with the limited imaging resolution and reduced off-axis interference rejection. The concept is to construct a picture by delaying the received signals from each aperture channel and summing resulting values. Weights are assigned to the received signals based on the receiving element's location, giving larger weights for central element signals, while elements located further out from the center are given lower weights [8]. By reducing the sidelobe level, this apodization operation improves imaging quality. The weight of apodization is constant and independent on data and has the disadvantage of broadening the mainlobe and decreasing lateral resolution [8]. Therefore, adaptive beamforming was developed. The minimum variance (MV) beamformer is an adaptive beamformer, which Capon pioneered in 1969. It is so named because it minimizes the output power, which is used to calculate the weighting vector while conserving the focal point response. Over the years, several strategies for enhancing MV beamformers have been presented. Mann proposes the frost beamformer in 2002 [13]. Sasso and Cohen-Bacrie proposed the spatial smoothing technique for decorrelating signals on and off the axis, as well as a well-conditioned covariance matrix [14]. Synnevg et al. used diagonal loading in estimating the covariance matrix [15]. In addition, they suggested a temporal averaged MV beamformer, where temporal averaging and spatial smoothing were utilized to preserve speckle statistics [15]. In MV, resolution is significantly improved compared to DAS, but contrast is still unsatisfactory. Here is where Eigenspace-based methods are introduced. The working assumption is to divide the covariance matrix into two orthogonal subspaces, signal and noise. The signal subspace describes the mainlobe signals information, while the noise subspace matches the sidelobe and off-axis signals [16, 17]. Asl and Mahloojifar presented eigenspace-based minimum variance (ESBMV) beamformer approach, which tells that the beamformer weights are obtained by projecting the MV weights onto the generated signal subspace [17, 18]. With using this method, the contrast is significantly improved, at the expense of presenting artificial dark spots called black-box regions (BBRs) at the sides of hyperechoic targets and the background speckle. In 2017, the partial-ESBMV (PESBMV) method was proposed to overcome the limitation of ESBMV. This method states that according to the signal subspace's eigenvector number, ESBMV is applied or blocked. This method thus managed to reduce BBR artifacts [8], but the contrast is decreased compared to ESBMV. After that, several methods were suggested to improve ESBMV's performance such as short-lag spatial coherence combined with ESBMV proposed to remove BBR artifacts under a high threshold of eigenvalues [19]. Also, ESBMV has been combined with Delay Multiply-And-Sum (DMAS) beamformer to decrease sidelobes level and increase the signal-to-noise ratio, this could not remove ESBMV's artifact [20]. It was also suggested to combine ESBMV with the sign coherence factor to improve the signal-to-noise ratio, but dark spots and BBRs still exist [21].

This paper presents a new method which is an upgraded version of the PESBMV. This method divides the imaging region into four areas based on their properties that directly affect the weight produced by ESBMV, in addition to the number of eigenvectors in the signal subspace matrix in ESBMV. This discrimination helps to use the beamforming technique that suits each region, resulting in improved overall ultrasound image quality.

2 Background Methods

2.1 Minimum Variance Beamformer (MV)

The weighting vector in an MV beamformer is always reorganized to minimize the output power through keeping unity gain for the response from the focal point, this requirement can be mathematically explained as [14, 15, 22]:

$$\mathbf{w}_{\mathrm{MV}} = \arg\min_{\mathbf{w}} \mathbf{w}^H \mathbf{R}\mathbf{w} \text{ subject to } \mathbf{w}^H\mathbf{a} = 1, \quad (1)$$

where the weighting vector is $\mathbf{w}$, $\mathbf{R}$ is the echo data's covariance matrix, $\mathbf{a}$ is defined as the steering vector accustomed to recompense for the delays from the focal point for each receiving element. The result is presented as [15, 22]:

$$\mathbf{w}_{\mathrm{MV}} = \frac{\mathbf{R}^{-1}\mathbf{a}}{\mathbf{a}^H\mathbf{R}^{-1}\mathbf{a}}. \quad (2)$$

The analytical form of $\boldsymbol{R}$ is unknown and is typically estimated from the data. In spatial smoothing where the element transducer array is divided into $\boldsymbol{P}$ subarrays, every subarray is identical to its neighboring subarray, however with one element shifted [23] Temporal smoothing, where $(2K + 1)$ is a vector of length-selected samples for each focal point [24] is included in the $\boldsymbol{R}$ calculation. The covariance matrix can be expressed as [15, 22]:

$$\boldsymbol{R} = \frac{1}{P}\sum_{P=0}^{P-1} G_p G_p^H, \quad (3)$$

where the number of subarrays is p, and it equals $(M - Lp + 1)$, where Lp is the length of the subarray in the spatial smoothing operation and M is the overall number of transducer elements. G_p is the p^{th} subarray, as follows [15, 22]:

$$G_p = \begin{bmatrix} y_p(n) & y_{p+1}(n) & \dots & y_{p+L_p-1}(n) \end{bmatrix}', \quad (4)$$

where $y_p(n)$ is a segment of the received input signal p^{th} element, $p = 0, 1, \dots, P-1$. $y_p(n)$ represents a vector of length $(2K + 1)$. The beamformer's output value is computed by multiplying the subarray average by the weighting vector [15, 22]:

$$Y = w_{MV}{}' \frac{1}{P} \sum_{p=0}^{P-1} G_p. \quad (5)$$

By studying the change of the value of Lp (Spatial smoothing technique with subarray length) on the contrast and resolution in MV and ESBMV methods, it is observed that a decreasing in the value of Lp leads to the lower contrast ratio, and contrast to noise ratio (approach to DAS beamforming method), and also decreases resolution and increases brightness, while the background speckle appears homogeneous and clear, one the other side the increase in the Lp value has a very positive and noticeable effect on the resolution and contrast but at the expense of reducing homogeneity of background speckle.

2.2 Eigen Space Based Minimum Variance (ESBMV)

The MV covariance matrix ($\boldsymbol{R}$) is separated into signal and noise subspaces, with a weighting vector projected to signal subspace. $\boldsymbol{R}$ can be written as following [27, 28]:

$$\boldsymbol{R} = \boldsymbol{V}\boldsymbol{\Lambda}\boldsymbol{V}^{\mathrm{H}} = \sum_{i=1}^{Lp} \lambda_i \boldsymbol{v}_i \boldsymbol{v}_i^{\mathrm{H}}, \quad (6)$$

where the diagonal matrix is $\boldsymbol{\Lambda} = \mathrm{diag}[\lambda_1, \lambda_2, \dots, \lambda_{Lp}]$, $\boldsymbol{R}$'s eigenvalues are represented by the diagonal., where $\lambda_1 \geqslant \lambda_2 \geqslant \cdots \geqslant \lambda_{Lp}$ are arranged in decreasing order. $V = [v_1, v_2, \dots, v_{Lp}]$ where $\boldsymbol{v}_i$ is the i^{th} orthonormal eigenvector for λ_i with $i = 1, \dots, Lp$. In this method, $\boldsymbol{R}$ is divided based on its Eigen structure, into signal and noise subspaces. Subsequently, the MV weighting vector is planned onto the corresponding subspace-constructed signal. As a result of the high coherency of on-axis signals, the energy produced by the mainlobe is focused on the eigenvectors related to the larger eigenvalue. Thus, the signal subspace matrix (E_s) is written as following [18]:

$$E_s = [v_1, v_2, \dots, v_{Num}], \quad (7)$$

where Num is the number of eigenvectors included in the signal subspace. The signal subspace is constructed from the eigenvectors whose corresponding eigenvalues are greater than δ times the highest eigenvalue (λ_{max}), where δ is a value of 0 to 1 and is set by the user [29]. New weights are then calculated by projecting the MV weight to the signal subspace using the following Eq. [18]:

$$\boldsymbol{w}_{ESBMV} = \boldsymbol{E}_s \boldsymbol{E}_s^{\mathrm{H}} \boldsymbol{w}_{MV}. \quad (8)$$

2.3 Partial Eigenspace-Based Minimum Variance (PESBMV)

Contrast and resolution in MV adaptive beamformers are improved by ESBMV beamforming. Nevertheless, two types of artifacts limit the execution of ESBMV. Firstly, BBR around hyperechoic targets, and secondly dark spots in background speckles. Therefore, PESBMV was proposed to overcome those limitations. By depending on the value of Num, this method can distinguish or divide the image into two areas. The first area contains hyperechoic objects, wires, and sidelobe and, the second area contains hypoechoic objects and speckle backgrounds. The weight in this method can be written as following [8]:

$$W_{PESBMV} = \begin{cases} E_s E_s^H w_{MV} & \text{if } Num > L_p.\eta \\ w_{MV} & \text{otherwise.} \end{cases}, \quad (9)$$

where η is a user-specified coefficient that varies between 0 and 1. PESBMV was able to achieve a quantum leap in the PWI field by averting the BBR artifacts and controlling the dark spots through changing the value of η .

2.4 Coherence Factor (CF)

The coherence factor (*CF*) method is frequently used to describe the superiority of adaptive imaging focusing [26]. *CF* is defined as following [27, 28]:

$$CF(k) = \frac{\left|\sum_{l-1}^{L} x_l(k)\right|^2}{M \sum_{l-1}^{L} |x_l(k)|^2}, \quad (10)$$

where $x_l(k)$ represents the data received from channel l after applying focusing delay and k is the time index. In ultrasonic imaging, CF value is commonly utilized as a weight to curb sidelobes. The ultimate beamformed output is found by following [26]:

$$y_{CF} = CF.Y. \quad (11)$$

2.5 Proposed Methods

The new method is proposed to maintain high imaging quality. It depends on the value of Num and the weight of ESBMV to distinguish between the regions. This method is proposed to take advantage of the properties of ESBMV in terms of contrast and MV in terms of reversing the homogeneous background speckle.

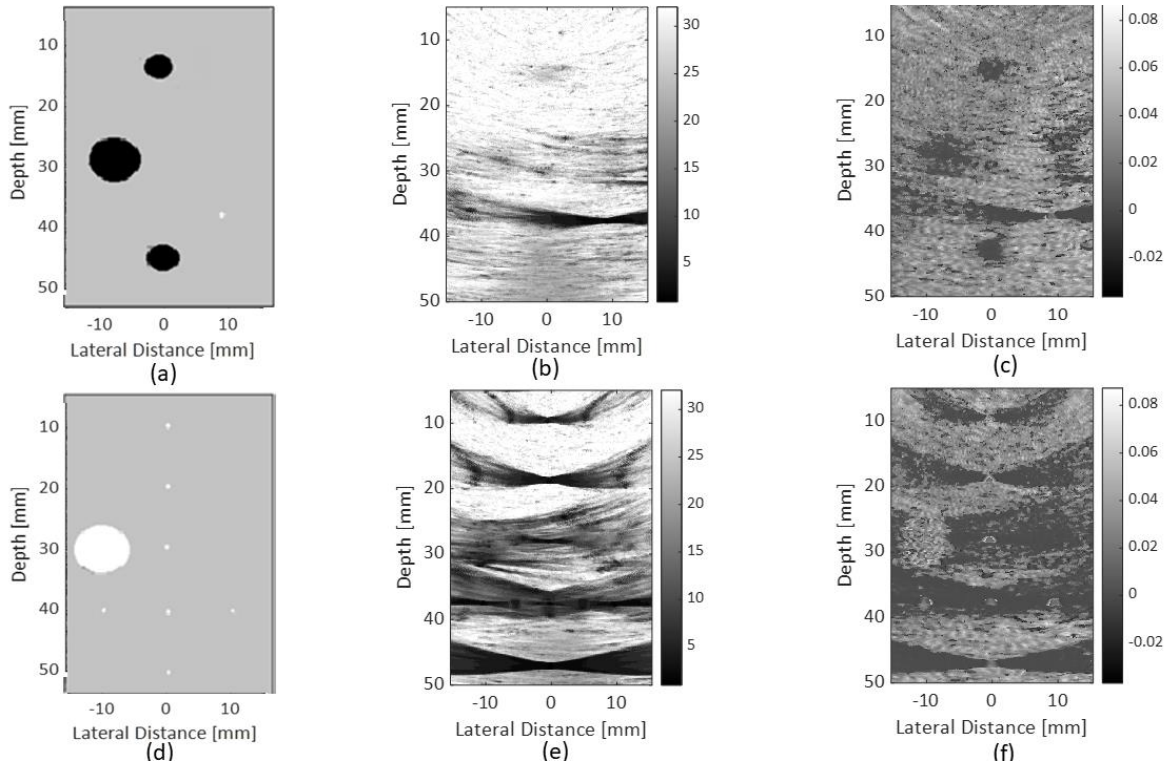

Fig. 1 The value of *Num*, using reference ESBMV at δ = 0.2, *Lp* = 32 in panel (b) for contrast phantom shown in panel (a) and panel (e) for resolution phantom shown in panel (d). Panel (a) shows a contrast phantom with three cysts centered at the 15 mm and 42 mm depths; panel (d) shows a resolution phantom with 7 wires hyperechoic lesion centered at the 26 mm depth. Panels (c) and (f) show the weight of ESBMV at δ= 0.2, *Lp* = 32 using contrast and resolution phantoms, respectively.

The idea is to exploit the positives of all the previously used methods and depending on specific values that discriminate and detect different areas of the image, the best performance of the methods is included in each region to obtain a high-quality image.

In this paper, two factors are proposed to distinguish between the different areas of the image. The first parameter is the value of Num by which the image is divided into two parts, the first is hyperechoic targets and sidelobe regions, and the second part is the hypoechoic target and background speckle. Afterwards, each of these two regions is further discriminated depending on the weight produced by ESBMV and on Num. The behavior of those two discrimination factors is emphasized in Fig. 1.

After discrimination, the proposed method uses ESBMV$(Lp = M/2)$ multiplied by *CF* for hypoechoic target, and MV $(Lp = 1)$ for background speckle and hyperechoic target regions.

Finally, MV $(Lp = M/2)$ is used for areas that include BBRs. The flow chart that explains the steps followed by this method is shown in Fig. 2.

The hyperechoic target is distinguished by observing the Num value, which is equal to one, as shown in Fig. 1. Also, the differentiation between the hypoechoic and background speckle was performed through the observation of the normalized ESBMV weight at $(Lp = M/4)$, which ranges between zero to 0.5 at hypoechoic targets, and between 0.5 to one at the background speckle.

3 Implementation and Experimental Datasets

3.1 Experimental Datasets

Ultrasound imaging quality is highly affected by the imaging parameters and settings, such as the type and width of the transducer, central frequency, bandwidth, etc. [29]. Therefore, the proposed beamforming method is tested and compared to standard beamformers under fixed imaging settings.

Two experimental datasets are used in this work. Those datasets were obtained from the web platform of the International Ultrasound Symposium IEEE 2016 held in Tours (France) [30]. A Verasonics Vantage 256 research scanner and an L11 probe were used to collect data (Verasonics Inc., Redmond, WA). CIRS Multi-Purpose Ultrasound Phantom (Model 040GSE) was used to collect the datasets as shown in Figs. 1(a) and (d) [31]. The first dataset is shown in Fig. 1(a) and has three anechoic cysts against a background speckle. The second dataset is shown in Fig. 1(d) [6]. The Matlab program is used to implement the proposed method as well as MV, ESBMV, and PESBV methods for assessment and compression. Table 1 gives the detailed settings used through data acquisition.

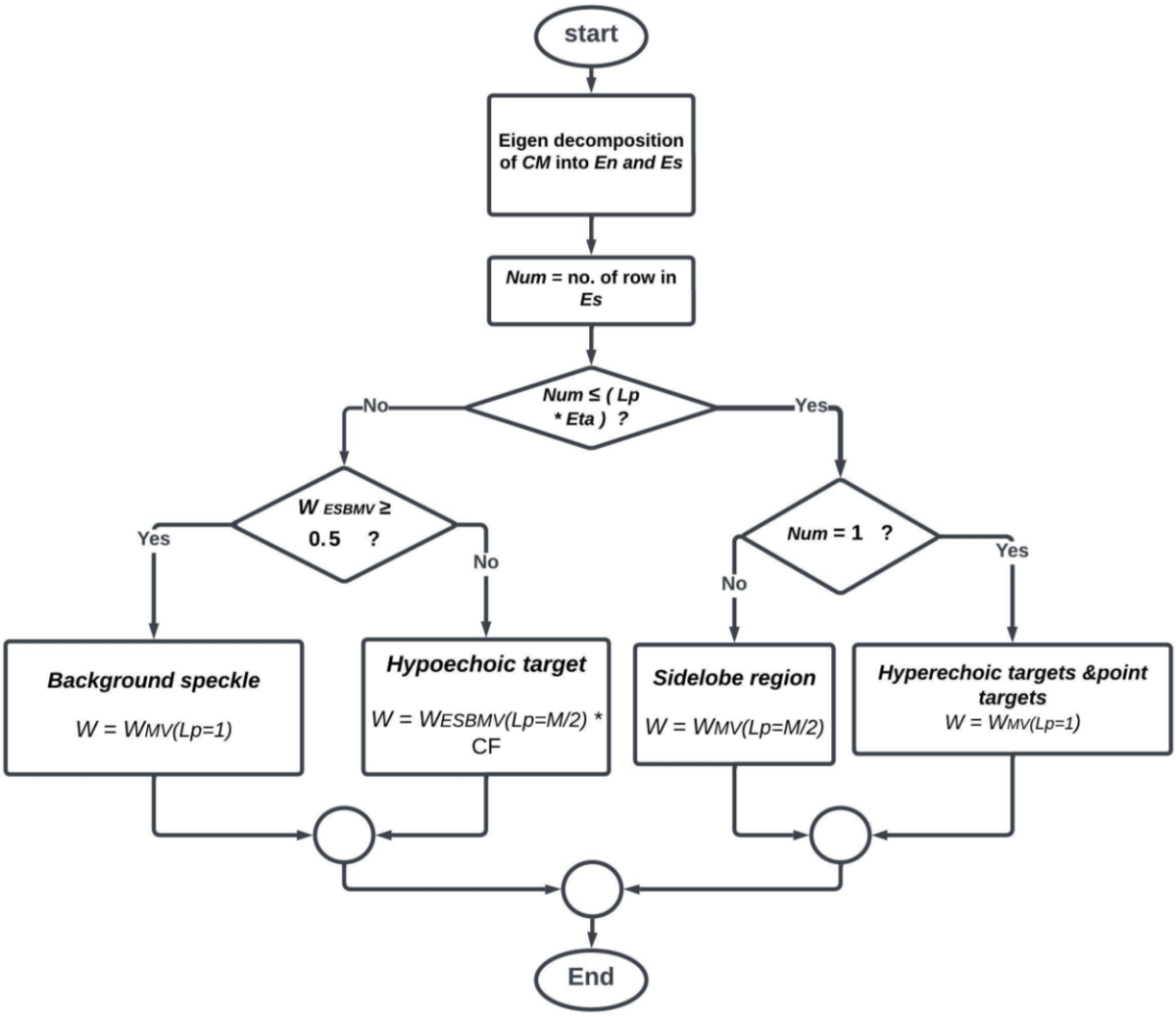

Fig. 2 Flow chart outlining the steps followed by the proposed method.

Table 1 The imaging settings employed during data acquisition.

Pitch	0.30 mm
Element width	0.27 mm
Element height	5 mm
Elevation focus	20 mm
Number of elements	128
Aperture width	38.4 mm
Transmit frequency	5.208 MHz
Sampling frequency	20.832 MHz
Pulse bandwidth	67%
Excitation	Cycles

3.2 Quality Metrics

In this section, well-known qualities for quantitative analyses of beamforming performance was used. Those metrics are contrast ratio (CR), contrast-to-noise ratio (CNR), speckle-to-noise ratio (SSNR), and full width at half maximum (FWHM).

CR indicated in the following equation. CR is used to evaluate imaging contrast; CR is determined from the absolute difference between the cystic area's mean value and the background tissue [32]:

$$CR = |\mu_i - \mu_b|, \tag{12}$$

where the mean values within the cyst target and speckle are μ_i and μ_b, respectively.

CNR is another measure of contrast that is found as follows [32]:

$$CNR = \frac{|\mu_i - \mu_b|}{\sqrt{\sigma_i^2 + \sigma_b^2}}, \tag{13}$$

where σ_i and σ_b are the equivalent standard deviations, within the cyst target and the speckle background, respectively. Two 2×1 squares inside cysts with two 11×15mm squares to the left and right above corner of the image are the background areas against which CR and CNR are calculated.

Table 2 Measurements of contrast and speckle statistics for the contrast phantom using different beamforming techniques with PWI.

Method	FWHM (mm)	CR (dB)	CNR (dB)	SSNR
MV (Lp = 1)	0.87	12.36	2.05	1.74
MV (Lp = M/2)	1	11.85	1.97	1.65
ESBMV (Lp = M/4)	0.77	15.67	2.44	1.63
ESBMV (Lp = M/2)	0.9	17.17	2.12	1.30
PESBMV (δ = 0.2, η = 0.5)	1.1	15.57	2.42	1.63
Proposed method (δ = 0.2, η = 0.5)	0.57	16.26	2.55	1.7

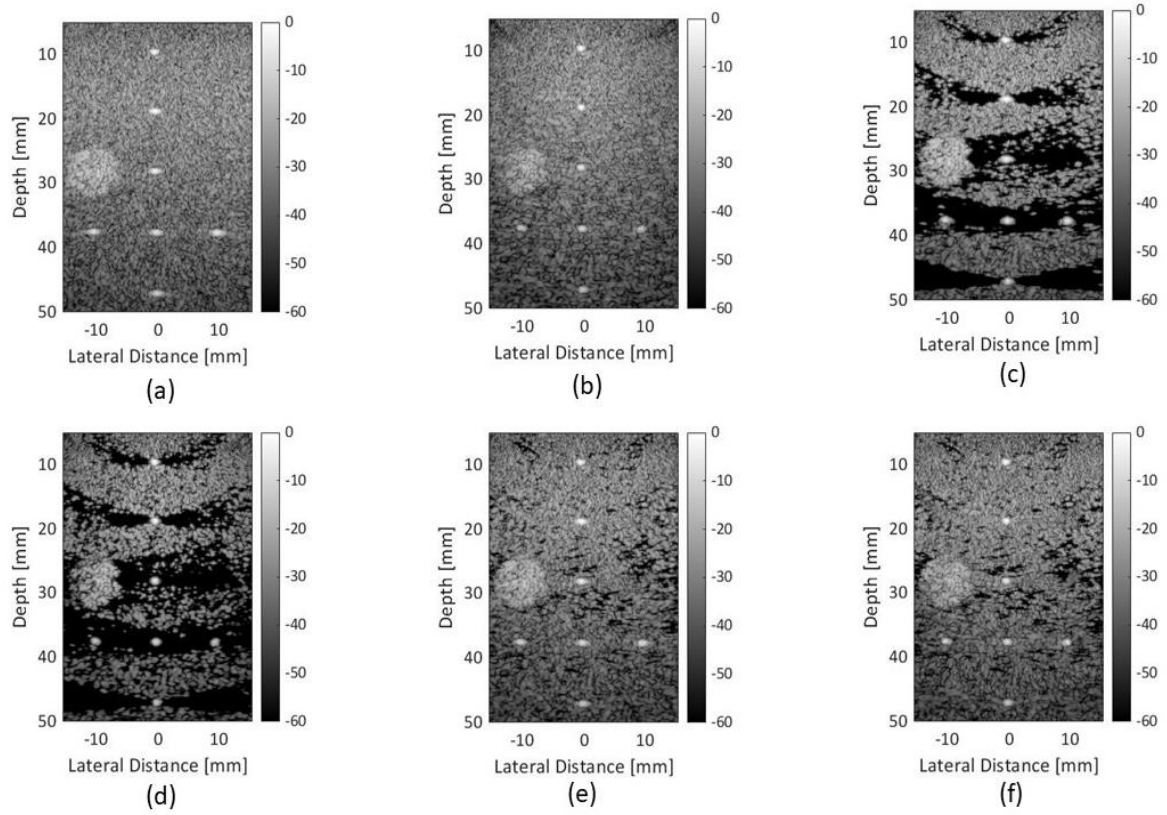

Fig. 3 Images of the experimental RF data of the resolution phantom using: (a) MV ($Lp = 1$), (b) MV ($Lp = M/2$), (c) ESBMV (δ = 0.2 , $Lp = M/4$), (d) ESBMV (δ = 0.2, $Lp = M/2$), (e) PESBMV (δ = 0.2, η = 0.5, $Lp = M/4$), and (f) proposed method (δ = 0.2, η = 0.5). All images are shown in a dynamic range of 60 dB.

Speckle signal to noise ratio (SSNRBg) is used to evaluate the quality of speckles. The following Eq. is used to determine $SSNR_{Bg}$ [33, 34]:

$$SSNR_{Bg} = \frac{\mu_b}{\sigma_b}, \quad (14)$$

In contrast phantom, 11 × 17 mm square in the right top corner is used to measure the background speckle's homogeneity using $SSNR_{Bg}$. As shown in Eq. (15), a similar formula is used to calculate the BBR's speckle-signal-to-noise-ratio ($SSNR_{BBR}$) [33, 34]:

$$\mathrm{SSNR}_{BBR} = \frac{\mu_{BBR}}{\sigma_{BBR}}, \quad (15)$$

where μ_{BBR} and σ_{BBR} are the BBR's mean and standard deviation values. In the resolution phantom, two 2 × 2mm to the sides of the wire target at a depth of 9 mm indicates the area for which, BBR artifacts are measured using $SSNR_{BBR}$.

Calculating the FWHM (6-dB beamwidth) of the main lobe in the lateral direction gives the lateral resolution [35].

4 Results and Discussion

In this work, a variety of beamformers is applied to the used datasets to evaluate the proposed beamformer's performance. Fig. 4 displays the superiority of the

proposed method in improved CR, where, as shown in Fig. 4(a) and (b) MV ($Lp = 1$), MV ($Lp = M/2$) respectively produce blurred boundaries for the anechoic cyst target. While there is visible noise in ESBMV ($Lp = M/4$), ESBMV ($Lp = M/2$), and PESBMV ($Lp = M/4$) decrease CR compared to ESBMV ($Lp = M/4$) as shown in Table 2.

The speckle pattern produced by MV ($Lp = M/2$) as shown in Fig. 4(b) is sandy and inhomogeneous, with significantly darker speckle intensity, while in the ESBMV method, the background speckle suffers from BBR. The PESBMV method is better than ESBMV in limiting dark spots and BBR. Nevertheless, the background speckle is very homogeneous using MV ($Lp = 1$ and $M/2$) as in Fig. 4 (a) and (b). This is comparable to DAS. Table 2 indicates that SSNR for the proposed method and MV ($Lp = 1$) is close, this illustrates the strength of proposed method in preserving the homogeny of speckle background.

Lateral responses of the implemented beamformers for the point target positioned at the 18.75 mm depth in the resolution phantom dataset are given in Fig. 5 and Fig. 3 to aid intuitive observations of their lateral resolution performance. The graphs show that when Lp increases, all MV-based methods considerably assist in reducing main lobe widths, where, compared to the other approaches, MV ($Lp = 1$) is less effective in improving lateral resolution since its main lobe width is similar to that of DAS. Fig. 5 shows that the worst resolution was achieved by ESBMV ($Lp = M/4$) but improved when increase Lp, as well as MV, lateral resolution in PESBMV approach from ESBMV method, form Table 2 it can be noticed that the smallest value of FWHM has been achieved using proposed method, with an improvement by (52%) compared the resolution achieved using PESBMV.

The presented algorithm is shown to be highly effective in increasing the quality of imaging by improving image contrast and speckle pattern preservation, as well as significantly increasing lateral resolution. This is done by sensing the details of the image first through the value of Num, which can efficiently distinguish hyperechoic targets and sidelobe regions from the rest of the regions, as it gives a value (1) for the hyperechoic target and greater than one to BBR as shown in Figs. 1(b) and (e), and secondly, using the value of the weights of ESBMV ($Lp = M/4$). This is because the values of this weight given to the cyst range from (0−0.5), as can be noticed in Figs. 1(c) and (f).

Fig. 4 illustrates that the cyst is much more visible using proposed method and that the proposed beamformer significantly improves CNR, exceeding all the implemented beamforming methods. Fig. 4 illustrates that the cyst is much more visible using proposed method and that the proposed beamformer significantly improves CNR, exceeding all the implemented beamforming methods. The main reason for that is the ability of the proposed method to detect the areas of the cysts. Second, the use of the CF justifies the weight of beamformer based on the incoherency of these signals.

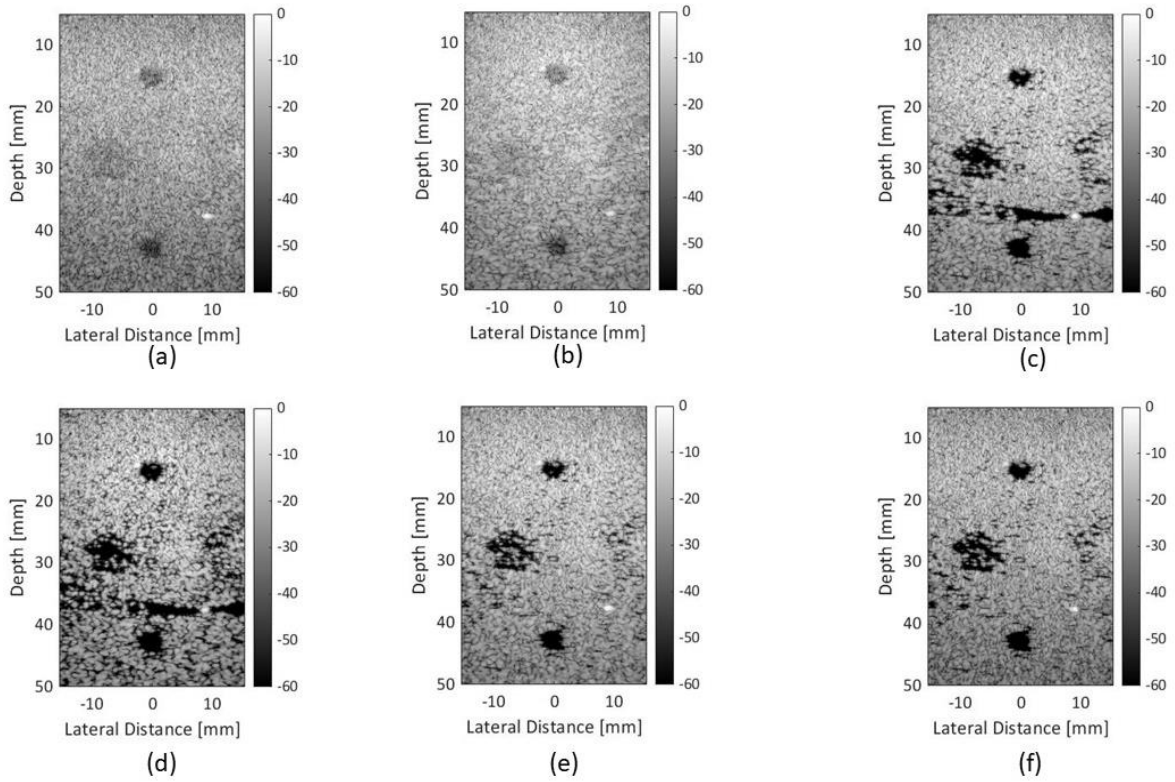

Fig. 4 Images of the experimental RF-data of cyst phantom using: (a) MV ($Lp = 1$), (b) MV ($Lp = M/2$), (c) ESBMV ($\delta = 0.2$, $Lp = M/4$), (d) ESBMV ($\delta = 0.2, Lp = M/2$), (e) PESBMV ($\delta = 0.2$, $\eta = 0.5$, $Lp = M/4$), and (f) proposed method ($\delta = 0.2$, $\eta = 0.5$). All images are shown in a dynamic range of 60 dB.

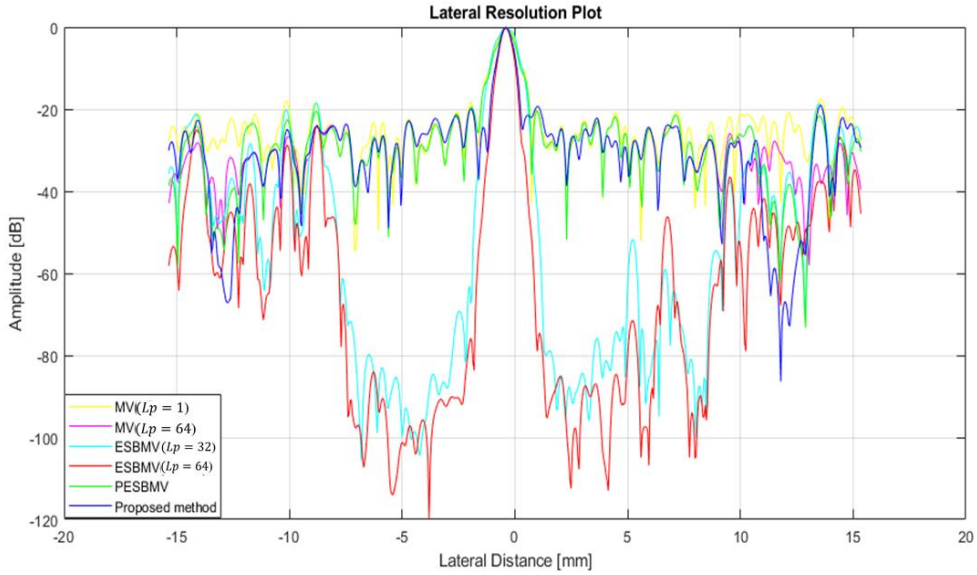

Fig. 5 FWHM displayed for the wire located at (z = 18.75 mm) depth of the dataset from resolution phantom.

Table 3 Measurements of black-box region and resolution for the resolution phantom using different beamforming techniques with PWI.

Method	FWHM (mm)	$SSNR_{BBR}$
MV ($\boldsymbol{Lp = 1}$)	1.086	5.82
MV ($\boldsymbol{Lp = M/2}$)	0.709	6.33
ESBMV ($\boldsymbol{Lp = M\ /4}$)	1.129	2.29
ESBMV ($\boldsymbol{Lp = M\ /2}$)	0.648	2.56
PESBMV ((δ = 0.2, η = 0.5)	0.987	6.03
Proposed method (δ = 0.2, η = 0.5)	0.704	5.89

Third reason is the projection of the MV weights onto the signal subspace also. Also, to improve speckle statistics and a contrast in tissue areas, temporal smoothing is applied, where a vector of samples instead of a single sample is used to produce the final value of the focal point.

The results presented in Table 2 confirm the superiority of the proposed method in terms of CR and CNR. When the weight of ESBMV ($Lp = M/4$) are higher than (0.5), this indicates inside the areas of the speckle. The proposed method uses MV ($Lp = 1$) because through it more homogenous background speckle and higher values of SSNR are achievable.

The issue of underestimation of the amplitude of hyperechoic targets when a large length of subarray is used has been solved by surrounding the hyperechoic and wire areas by MV ($Lp = M/2$) while giving the hyperechoic and wire targets weights of MV ($Lp = 1$). The results of this method were obtained as described in Table 2 and Table 3.

5 Conclusions

In this paper, we introduce a novel approach for improving image quality. The new algorithm which discriminates imaging area based on Num and the weight of ESBMV is meant to improve lateral resolution and speckle preservation while simultaneously increasing contrast by using different beamforming types in each defined area. Experimental results show that the proposed approaches can achieve increased image contrast and very well keep speckle patterns with a significant increase in lateral resolution. Additionally, the proposed approach has the potential to be an effective strategy for improving image quality in other imaging methods as well as Compound Plane Wave Imaging (CPWI).

Acknowledgments

The authors are grateful to the Department of Communications Engineering, Electronics Engineering College, Ninevah University on their unlimited support during conducting this research.

Disclosures

The authors declare no conflict of interest.

References

1. I. Edler, K. Lindström, "The history of echocardiography," Ultrasound in Medicine & Biology 30(12), 1565–1644 (2004).
2. V. Chan, A. Perlas, "Basics of ultrasound imaging," in Atlas of Ultrasound-Guided Procedures in Interventional Pain Management, S. N. Narouze (Ed.), 13–19 (2011).
3. J. Bercoff, M. Tanter, and M. Fink, "Supersonic shear imaging: a new technique for soft tissue elasticity mapping," IEEE Transactions on Ultrasonics, Ferroelectrics, and Frequency Control 51(4), 396–409 (2004).
4. J. Bercoff, G. Montaldo, T. Loupas, D. Savery, F. Mézière, M. Fink, and M Tanter, "Ultrafast compound Doppler imaging: Providing full blood flow characterization," IEEE Transactions on Ultrasonics, Ferroelectrics, and Frequency Control 58(1), 134–47 (2011).
5. J. T. Ylitalo, H. Ermert, "Ultrasound synthetic aperture imaging: monostatic approach," IEEE Transactions on Ultrasonics, Ferroelectrics, And Frequency Control 41(3), 333–339 (1994).
6. H. Liebgott, A. Rodriguez-Molares, F. Cervenansky, J. A. Jensen, and O. Bernard, "Plane-wave imaging challenge in medical ultrasound," 2016 IEEE International Ultrasonics Symposium (IUS), O. Minin (Ed.), InTechOpen (2016).
7. J. Bercoff, "Ultrafast ultrasound imaging," Chapter 1 in Ultrasound Imaging-Medical Applications, I. V. Minin, O. V. Minin (Ed.), InTeach, 3–24 (2011).
8. Z. R. S. Alomari, "Plane Wave Imaging Beamforming Techniques for Medical Ultrasound Imaging," PhD Thesis, University of Leeds (2017).
9. M. Tanter, M. Fink, "Ultrafast imaging in biomedical ultrasound," IEEE Transactions on Ultrasonics, Ferroelectrics, and Frequency Control 61(1), 102–19 (2014).
10. K. Ranganathan, W. F. Walker, "A novel beamformer design method for medical ultrasound. Part I: Theory," IEEE Transactions on Ultrasonics, Ferroelectrics, and Frequency Control 50, 15–24 (2003).
11. G. Matrone, A. S. Savoia, G. Caliano and G. Magenes, "The delay multiply and sum beamforming algorithm in ultrasound B-mode medical imaging," IEEE Transactions on Medical Imaging 34(4), 940–9 (2014).
12. K. E. Thomenius, "Evolution of ultrasound beamformers," Proceedings of 1996 IEEE Ultrasonics Symposium 2, 1615–1622 (1996).
13. J. A. Mann, W. F. Walker, "A constrained adaptive beamformer for medical ultrasound: Initial results," Proceedings of 2002 IEEE Ultrasonics Symposium 2, 1807–1810 (2002).
14. M. Sasso, C. Cohen-Bacrie, "Medical ultrasound imaging using the fully adaptive beamformer," IEEE International Conference on Acoustics, Speech, and Signal Processing 2, 489–492 (2005).
15. J. F. Synnevag, A. Austeng, and S. Holm, "Adaptive beamforming applied to medical ultrasound imaging," IEEE transactions on Ultrasonics, Ferroelectrics, and Frequency Control 54(8), 1606–1613 (2007).
16. J. L. Yu, C. C. Yeh, "Generalized eigenspace-based beamformers," IEEE Transactions on Signal Processing 43, 2453–2461 (1995).
17. X. Zeng, C. Chen, and Y. Wang, "Eigenspace-based minimum variance beamformer combined with Wiener postfilter for medical ultrasound imaging," Ultrasonics 52(8), 996–1004 (2012).
18. B. M. Asl, A. Mahloojifar, "Eigenspace-based minimum variance beamforming applied to medical ultrasound imaging," IEEE Transactions on Ultrasonics, Ferroelectrics, and Frequency Control 57(11), 2381–2390 (2010).
19. Y. Wang, C. Zheng, H. Peng, and X. Chen, "Short-lag spatial coherence combined with eigenspace-based minimum variance beamformer for synthetic aperture ultrasound imaging," Computers in Biology and Medicine 91, 267–276 (2017).
20. M. Mozaffarzadeh, A. Mahloojifar, V. Periyasamy, M. Pramanik, and M. Orooji, "Eigenspace-based minimum variance combined with delay multiply and sum beamformer: Application to linear-array photoacoustic imaging," IEEE Journal of Selected Topics in Quantum Electronics 25(1), 1–8 (2018).
21. S. Shamekhi, V. Periyasamy, M. Pramanik, M. Mehrmohammadi, and B. M. Asl, "Eigenspace-based minimum variance beamformer combined with sign coherence factor: Application to linear-array photoacoustic imaging," Ultrasonics 108, 106174 (2020).
22. I. K. Holfort, F. Gran, and J. A. Jensen, "Broadband minimum variance beamforming for ultrasound imaging," IEEE Transactions on Ultrasonics, Ferroelectrics, and Frequency Control 56, 314–325 (2009)
23. T. J. Shan, T. Kailath, "Adaptive beamforming for coherent signals and interference," IEEE Transactions on Acoustics, Speech, and Signal Processing 33(3), 527–536 (1985).
24. Synnevåg J-F, Nilsen C-I and Holm S 2007 P2b-13 speckle statistics in adaptive beamforming 2007 IEEE Ultrasonics Symposium Proceedings (IEEE) pp 1545–8
25. S. Mehdizadeh, A. Austeng, T. F. Johansen and S. Holm, "Eigenspace based minimum variance beamforming applied to ultrasound imaging of acoustically hard tissues," IEEE Transactions on Medical Imaging 31(10), 1912–1921 (2012).
26. K. W. Hollman, K. W. Rigby, and M. O'donnell, "Coherence factor of speckle from a multi-row probe," IEEE Ultrasonics Symposium. Proceedings. International Symposium 2, 1257–1260 (1999).

27. C. I. C. Nilsen, S. Holm, "Wiener beamforming and the coherence factor in ultrasound imaging," IEEE Transactions on Ultrasonics, Ferroelectrics, and Frequency Control 57(6), 1329–1346 (2010).
28. B. M. Asl, A. Mahloojifar, "Minimum variance beamforming combined with adaptive coherence weighting applied to medical ultrasound imaging," IEEE Transactions on Ultrasonics, Ferroelectrics, and Frequency Control 56, 1923–1931 (2009).
29. Z. Alomari, S. Harput, S. Hyder, and S. Freear, "The effect of the transducer parameters on spatial resolution in plane-wave imaging," IEEE International Ultrasonics Symposium (IUS) 1–4 (2015).
30. Plane-wave Imaging Challenge in Medical UltraSound (PICMUS), 1 April 2016 (accessed 22 January 2023). [https://www.creatis.insa-lyon.fr/Challenge/IEEE_IUS_2016/].
31. Multi-Purpose Multi-Tissue Ultrasound Phantom (CIRS), 12 December 2022 (accessed 10 December 2023). [https://www.cirsinc.com/products/ultrasound/zerdine-hydrogel/multi-purpose-multi-tisse-ultrasound-phantom/].
32. C. H. Seo, "Improved contrast in ultrasound imaging using dual apodization with cross-correlation," PhD Thesis, University of Southern California (2008).
33. M. A. Lediju, G. E. Trahey, B. C. Byram, and J. J. Dahl, "Short-lag spatial coherence of backscattered echoes: Imaging characteristics," IEEE Transactions on Ultrasonics, Ferroelectrics, and Frequency Control 58, 1377–1388 (2022).
34. M. Xu, X. Yang, M. Ding, and M. Yuchi, "Spatio-temporally smoothed coherence factor for ultrasound imaging [correspondence]," IEEE Transactions on Ultrasonics, Ferroelectrics, and Frequency Control 61(1), 182–190 (2014).
35. S. Harput, J. McLaughlan, D. M. J. Cowell, and S. Freear, "New performance metrics for ultrasound pulse compression systems," IEEE International Ultrasonics Symposium, 440–443 (2014).